JCBFM

Evaluation of single bolus, dual-echo dynamic susceptibility contrast MRI protocols in brain tumor patients

Ashley M Stokes[1] ⓘ, Maurizio Bergamino[1], Lea Alhilali[2], Leland S Hu[3], John P Karis[2], Leslie C Baxter[1,3], Laura C Bell[1] ⓘ and C Chad Quarles[1]

Abstract

Relative cerebral blood volume (rCBV) obtained from dynamic susceptibility contrast (DSC) MRI is adversely impacted by contrast agent leakage in brain tumors. Using simulations, we previously demonstrated that multi-echo DSC-MRI protocols provide improvements in contrast agent dosing, pulse sequence flexibility, and rCBV accuracy. The purpose of this study is to assess the *in-vivo* performance of dual-echo acquisitions in patients with brain tumors (n = 59). To verify pulse sequence flexibility, four single-dose dual-echo acquisitions were tested with variations in contrast agent dose, flip angle, and repetition time, and the resulting dual-echo rCBV was compared to standard single-echo rCBV obtained with preload (double-dose). Dual-echo rCBV was comparable to standard double-dose single-echo protocols (mean (standard deviation) tumor rCBV 2.17 (1.28) vs. 2.06 (1.20), respectively). High rCBV similarity was observed (CCC = 0.96), which was maintained across both flip angle (CCC = 0.98) and repetition time (CCC = 0.96) permutations, demonstrating that dual-echo acquisitions provide flexibility in acquisition parameters. Furthermore, a single dual-echo acquisition was shown to enable quantification of both perfusion and permeability metrics. In conclusion, single-dose dual-echo acquisitions provide similar rCBV to standard double-dose single-echo acquisitions, suggesting contrast agent dose can be reduced while providing significant pulse sequence flexibility and complementary tumor perfusion and permeability metrics.

Introduction

Relative cerebral blood volume (rCBV) measures obtained from dynamic susceptibility contrast-(DSC)-MRI are widely used in the diagnosis and treatment of brain tumors.[1,2] Unfortunately, contrast agent leakage effects are often observed in brain tumors, as well as other pathologies, limiting the reliability of rCBV measurements.[1,3] To reduce contaminating T_1 effects, current recommendations include preload administration of a single full dose of contrast agent, given 5–10 minutes before dynamic imaging, followed by a second full dose of contrast agent.[4] This protocol yields highly robust rCBV maps and excellent agreement across multi-site studies;[5] however, this double bolus strategy has multiple drawbacks, including

higher costs, longer protocol times, increased contrast dose, and the potential for increased protocol variability,[6,7] due to multiple timed injections. A single bolus scheme would reduce cost, scan times, and contrast

[1]Division of Neuroimaging Research, Barrow Neurological Institute, Phoenix, AZ, USA
[2]Neuroradiology, Southwest Neuroimaging at Barrow Neurological Institute, Phoenix, AZ, USA
[3]Department of Radiology, Division of Neuroradiology, Mayo Clinic Arizona, Phoenix, AZ, USA

Corresponding author:
Ashley M Stokes, Division of Neuroimaging Research, Barrow Neurological Institute, 350 W. Thomas Rd, Phoenix, AZ 85013, USA.
Email: ashley.stokes@barrowneuro.org

agent doses, while simultaneously simplifying and facilitating standardized clinical applications by eliminating multiple timed doses.

To that end, previous simulation studies using a patient-derived digital reference object (DRO) predicted that an optimized single-dose protocol with a specific set of parameters could provide rCBV accuracy comparable to the standard double-dose protocol.[8–10] This protocol is based on a low flip-angle (FA) acquisition, which reasonably balances T_1 and T_2* sensitivity to yield highly reliable rCBV measures with a single dose. In a multi-site study, Schmainda et al. validated this single bolus scheme,[11] demonstrating that a low FA single-dose protocol achieves rCBV values consistent with standard double-dose protocols acquired with a moderate FA (60–70°). However, DRO simulations also predicted that the high rCBV accuracy of low FA protocols is highly contingent upon a precise set of pulse sequence parameters. Any deviations from this protocol in terms of FA, echo times (TEs), and repetition times (TRs) lead to rapid decline of rCBV accuracy. This becomes problematic for simultaneous multi-slice acceleration methods, which have a shorter TR and are increasingly used in DSC perfusion to achieve higher temporal resolution. As single echo acquisitions are sensitive to contrast agent-induced changes in both T_1 and T_2*, rCBV accuracy in these protocols remains inherently tied to parameter variations. This has motivated efforts to develop highly accurate single-dose DSC-MRI protocols with more parameter flexibility.

In contrast to low-FA protocols that reduce T_1 leakage effects, multiple echo acquisitions have been shown to remove T_1 leakage effects.[3,12–15] Using DRO-based simulations, we recently demonstrated that multi-echo acquisitions provide high rCBV accuracy across over 2000 unique protocols, effectively decoupling both FA and TR from rCBV accuracy.[16] More specifically, we evaluated a wide array of multi-echo acquisitions (two dosing schemes, two field strengths, three TRs, three flip angles (FA), 29 echo time combinations, and with and without leakage correction) to demonstrate that multi-echo acquisitions, including dual-echo acquisitions, do not require a preload injection and provide significant pulse sequence flexibility without compromising rCBV accuracy. While DRO simulations suggest that a single bolus, dual-echo technique would provide equivalent rCBV values, this has never been evaluated in-vivo. Given the high rCBV accuracy for single-dose low-FA protocols due to reduced T_1 effects, we hypothesize that single-dose dual-echo protocols will similarly provide high rCBV accuracy by removing T_1 leakage effects, thus obviating the need for preload contrast doses. Additionally, dual-echo protocols enable quantification of dynamic T_1 changes, which can be used for simultaneous dynamic contrast enhanced (DCE) modeling. The purpose of this study is to assess the in-vivo performance of no preload (single-dose), dual-echo acquisitions compared to the standard preload (double-dose), single-echo protocol.

Material and methods

Subjects

This retrospective study was approved by the Dignity Health Institutional Review Board (IRB), and a waiver of informed consent was obtained. Data were acquired as part of the clinical standard of care over a two-year period between October 2017 and October 2019. Inclusion criteria included age over 18 years of age, presence of a brain tumor of any cellular origin, and availability of perfusion datasets for both preload and main injections on the institutional PACS. For patients with multiple available imaging datasets, only the first dataset per patient was used. Additional exclusion criteria included missing dynamic data points (n = 1), improper slice planning (n = 1), poor injection profiles (n = 3), and susceptibility artifact obscuring the region of interest (n = 2). The remaining subjects (n = 59) were further split into four groups based on the protocol used, as described below.

MRI protocol

All subjects underwent MRI at 3 T (Philips Ingenia, Best, Netherlands). Standard structural pre- and post-contrast T_1-weighted images were acquired using a 3 D magnetization-prepared rapid acquisition gradient echo (MP-RAGE) sequence with the following acquisition parameters: TR/TE, 7.9/4.4 ms; acquisition matrix, 256×256; voxel size, 1.0×1.0 mm^2; slice thickness, 1.0 mm; 170 sagittal slices; flip angle = 8°. Two consecutive DSC-MRI acquisitions (Table 1) were obtained during the administration of two contrast doses of a gadolinium-based contrast agent (gadobutrol, Gadavist). Both DSC acquisitions were acquired with spatial resolution of 1.75×1.75 mm^2 with slice thickness of 5 mm (acquisition matrix, 128×128); the pixel bandwidth for all DSC acquisitions was approximately 2 kHz. For both injections, the bolus was injected at 3 ml/s using a power injector after 30 seconds of baseline acquisition. During the first bolus, a dual-echo DSC protocol was performed (TE1/TE2 = 7.3/33.3 ms), thus allowing for evaluation of a single bolus (no preload, dual-echo) protocol and simultaneously serving as preload for the double bolus single-echo technique. After a delay of 6 minutes, a full-dose (0.1 mmol/kg) contrast bolus was injected during a standard single-echo DSC acquisition (TE = 30 ms, TR = 1.4 s, FA = 75° for all 59 patients), allowing

Table 1. Protocol description for each group.

Group[a]	n (59 total)	Bolus 1: Dual-echo protocol				Bolus 2: Single-echo protocol			
		TEs (ms)	Doseb	FA	TR (s)	TE (ms)	Dose	FA	TR (s)
Basic	15	7.33/33	1	75°	1.4	30	1	75°	1.4
$^1/_2$-dose	10	7.33/33	1/2	75°	1.4	30	1	75°	1.4
low FA	16	7.33/33	1	**30°**	1.4	30	1	75°	1.4
short TR	18	7.33/33	1	75°	**0.6**	30	1	75°	1.4

[a]Groups are defined based on the dual-echo protocol. [b]Dose given as 1 (= 0.1 mmol/kg) and $^1/_2$ (= 0.05 mmol/kg).

evaluation of a double bolus protocol in the same patient, during the same scan session as the single bolus/no preload protocol.

Over the two-year period of eligibility, four different protocols were used for the first bolus perfusion, including a basic protocol with full-dose contrast injection and moderate TR and FA (n = 15, basic protocol). Relative to the basic protocol, each of the remaining three protocols have a single modification: (1) $^1/_2$-dose contrast injection with moderate TR and FA (n = 10, $^1/_2$-dose protocol), (2) full-dose contrast injection with moderate TR and low FA (n = 16, low FA protocol), and (3) full-dose contrast injection with short TR and moderate FA (n = 18, short TR protocol) (see Table 1 for specific values). For the short TR protocol, the TR was reduced due to availability of simultaneous multi-slice (SMS) capabilities on the scanner. Each acquisition lasted for at least two minutes (2.1 minutes for the short TR protocol, and 2.8 minutes for the remaining protocols). Groups are defined based on their first bolus perfusion protocol, while the second bolus perfusion was consistent for all subjects.

Data analysis

The data that support the findings of this study are available from the corresponding author, AMS, upon reasonable request. Perfusion analysis was performed using in-house Matlab software (Mathworks), which is available upon request. The pre- and post-contrast images were registered using FLIRT (FSL) to the dual-echo images using the first echo time (averaged over dynamics). Although both perfusions were acquired with matching geometry, registration between the two perfusion datasets was performed using FLIRT, and all data were analyzed in the dual-echo perfusion space. Tumor region-of-interests (ROIs) were drawn covering the entire enhancing region from the ΔT_1 images (T_1w post-contrast – T_1w pre-contrast); in non-enhancing tumors (n = 8), tumor ROIs were drawn from the T_2w hyperintense regions. Normal-appearing white matter (NAWM) ROIs were drawn on the T_1w pre-contrast image.

More specifically, ROIs were drawn in uniform locations near the lateral ventricles (typically adjacent to the frontal or occipital horn of the lateral ventricle), on the side contralateral to the tumor ROI. All ROIs were drawn by an experienced researcher with 8 years of experience (AMS) and verified by a board-certified neuroradiologist with 14 years of experience in neuro-oncologic imaging (LSH), taking care to avoid both CSF and large vessels. The same tumor and NAWM ROIs were used for quantification of both sets of perfusion metrics (dual-echo and single-echo).

For dual-echo (first injection) and single-echo (second injection) data, ΔR_2^* was calculated using equations (1) and (2), respectively:

$$\Delta R_{2,DE}^*(t) = \frac{1}{(TE_2 - TE_1)} \left(\ln\left(\frac{S_{TE1}(t)}{S_{TE1}(0)}\right) - \ln\left(\frac{S_{TE2}(t)}{S_{TE2}(0)}\right) \right) \tag{1}$$

$$\Delta R_2^*(t) = -\frac{\ln\left(\frac{S(t)}{S(0)}\right)}{TE} \tag{2}$$

where $S(t)$ and $S(0)$ denote the dynamic signal and pre-bolus (baseline) signals, respectively, for each echo time (TE1 and TE2 for dual-echo, TE for single-echo). Equation (2) inherently assumes that T_1 signal contributions are negligible, while T_1 signal contributions are explicitly removed for dual-echo ΔR_2^* (equation (1)). Furthermore, the dynamic T_1-weighted signal contributions can be determined by extrapolating the dual-echo signal to TE = 0:

$$S_{TE=0} = S_{TE1} \left(\frac{S_{TE1}}{S_{TE2}}\right)^{\frac{TE1}{(TE2 - TE1)}} \tag{3}$$

Leakage correction was performed on both the single-echo and dual-echo data using the standard Boxerman-Schmainda-Weisskoff (BSW) method,[17,18] modified to account for both T_1 and T_2^* leakage effects.[19] The arterial input function (AIF) for each injection was determined using previously published

automated methods with specific dual-echo[20] and single-echo[21] criteria; subsequently, the AIF and tissue ΔR_2^* were converted to concentration using quadratic and linear relaxivity relationships, respectively.[22,23] CBV was determined using integration of the dynamic ΔR_2^* curve up to two minutes (up to 60 s each of baseline and post-injection), and negative values of ΔR_2^* were not included in the integration. Cerebral blood flow (CBF) was determined from the maximum of the impulse response function obtained from circular singular value decomposition (cSVD)[24] of the input AIF with the tissue ΔR_2^*, using an adaptive threshold.[25] CBV and CBF were normalized to normal-appearing white matter, yielding relative CBV (rCBV) and CBF (rCBF). The signal extrapolated to TE = 0 (equation (3), dual-echo first injection only) was used for DCE analysis,[26] using the extended Toft's model[27] with a separate DCE-based AIF[28] and a fixed T_1 value[29] of 1.5 s. Comparisons between dual-echo protocols with varying acquisition parameters (dose, TR, FA) and single-echo protocols (same protocol for all) were performed using the mean value over the tumor ROI; additionally, hot-spot analysis was performed using the 95th percentile within the tumor ROI.

To assess the dynamic signal characteristics for each protocol, temporal signal-to-noise ratio (tSNR) was calculated voxel-wise and averaged across the whole brain; additionally, the tumor contrast-to-noise ratio (CNR) was determined for each protocol. As the dual-echo acquisition comprises two signals, tSNR was determined from the ΔR_2^* curves (equations (1) and (2)). Specifically, tSNR was calculated as the ratio of peak ΔR_2^* to the standard deviation (SD) of the baseline ΔR_2^*. To assess lesion conspicuity for each protocol and injection, CNR was calculated as follows:

$$CNR = \frac{\mu_T - \mu_{NAWM}}{\sqrt{\sigma_T^2 + \sigma_{NAWM}^2}} \quad (4)$$

where μ_T and μ_{NAWM} indicates the mean tumor and NAWM rCBV, respectively, and σ_T and σ_{NAWM} indicates the standard deviation of tumor and NAWM rCBV, respectively.

Statistical analysis

Correlation analyses were performed in Matlab using Deming regression, which assumes measurement error occurs in both single-echo rCBV (x) and dual-echo rCBV (y). Concordance correlation coefficient (CCC) and Pearson's correlation coefficient (r) were used to assess ROI agreement and linearity, respectively. Concordance coefficients were interpreted as < 0.90: poor, 0.90 to 0.95: moderate, 0.95 to 0.99:

substantial, > 0.99 almost perfect.[30] Bland-Altman plots were used to assess bias (mean difference) and limits of agreement (LoA, = bias ± 1.96 x SD of bias). Statistical analyses were performed using RStudio V1.0.143 and R version 3.5.1. Data that were normally distributed (notably tSNR, CNR, and K^{trans}, as determined using Shapiro-Wilk tests) were compared using paired Student's t-tests or one-way analysis of variance (ANOVA), as specified below; data that were not normally distributed were compared using paired Wilcoxon signed rank or Kruskal-Wallis tests. More specifically, tSNR and CNR were compared between dual- and single-echo for each protocol (paired t-tests), and significance was determined using the false-discovery rate (FDR) correction for multiple comparisons. One-way ANOVA was performed to determine whether tSNR and CNR vary across protocols, while K^{trans} was compared across dual-echo protocols (one-way ANOVA with Tukey post-hoc comparisons). Perfusion metrics were compared between the dual- and single-echo protocols (first and second injection, respectively) for each parameter (rCBV: tumor mean and hot-spot; rCBF: tumor mean). As these parameters were non-normally distributed, per Shapiro-Wilk tests, paired Wilcoxon signed rank tests were used to compare parameters in each protocol. Kruskal-Wallis tests were used to determine whether rCBV varied across protocols, with Wilcoxon rank sum test for subsequent post-hoc comparisons using FDR correction for multiple comparisons. Results were considered significant at $p < 0.05$.

Results

A total of 59 subjects were identified that satisfied all inclusion/exclusion criteria. The average age was 51.3 years old (SD = 13.7, range = 27.0–88.0), and there were 31 males included. Most of the tumors were glial in origin (n = 51; 86%), the majority of which were high-grade (n = 39/51; 76%), followed by metastatic tumors (n = 5; 8.5%), meningiomas (n = 2; 3.4%), and mixed tumor types (n = 1; 1.7%). Additionally, most tumors demonstrated contrast enhancement (n = 51) on ΔT_1 images, where the remaining non-enhancing tumors (n = 8) were all low-grade gliomas. The subject and tumor characteristics for each of the four dual-echo protocol groups are shown in Table S1 (supplementary material).

Figure 1 shows the dual-echo (first injection, no preload) and single-echo (second injection, with preload) signals (top row) and ΔR_2^* curves (middle rows) in the tumor ROI, along with the automated AIFs, for each protocol. A smaller susceptibility-induced signal drop can be seen in the ½-dose dual-echo protocol. T_1 leakage effects are evident in the individual dual-echo
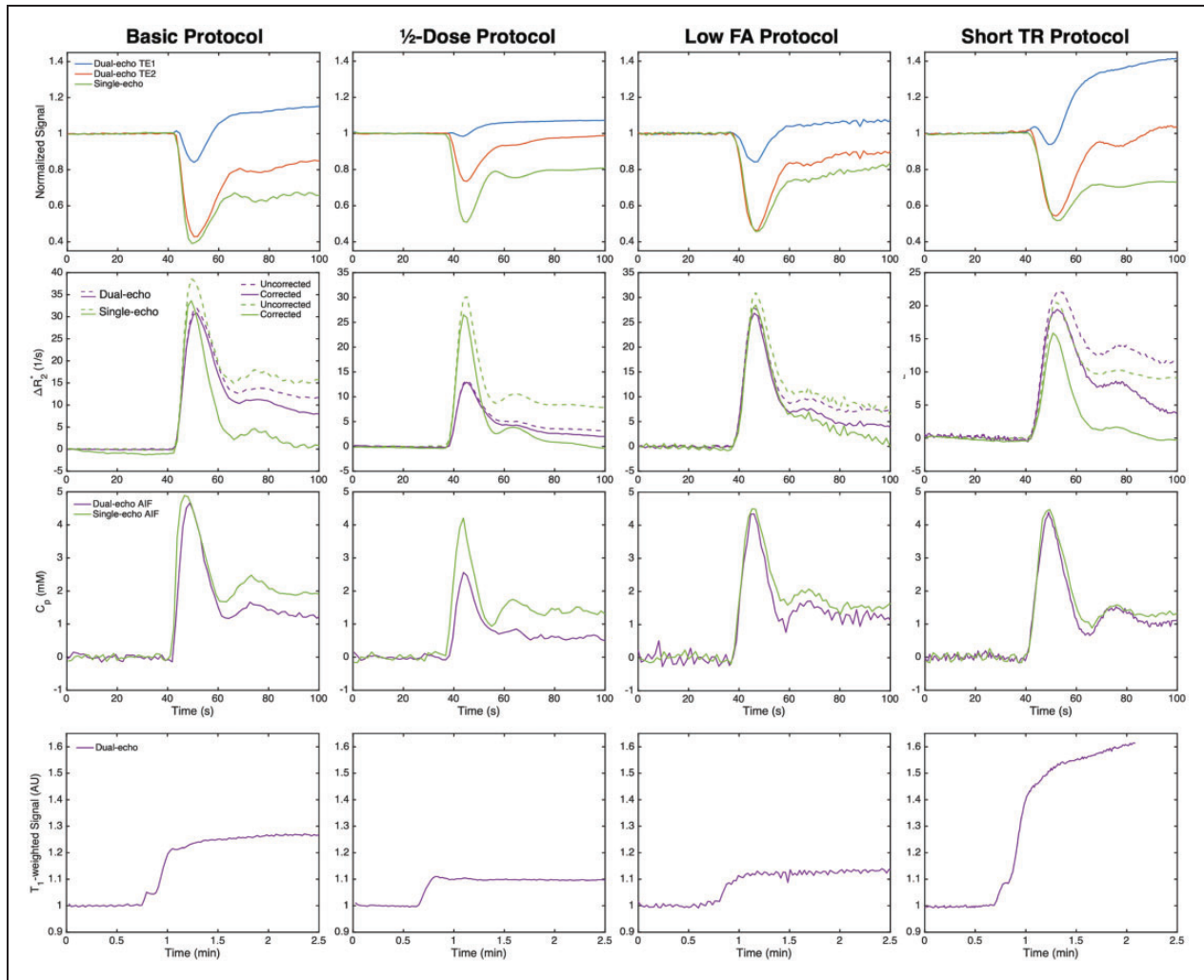
Figure 1. Top to bottom: Dual-echo (no preload) and single-echo (with preload) signals (normalized to baseline), ΔR_2^* curves in a brain tumor ROI, corresponding AIF, and tumor T_1-weighted curves (dual-echo only) for each protocol (left to right). All curves are from GBM patients. T_1 leakage effects can be observed in the signals for the dual-echo acquisition (particularly TE1), which are removed in the dual-echo ΔR_2^*.

signals, particularly in the first echo (blue) of protocols with parameters that induce higher T_1-weighting (higher FA and/or shorter TR). For the single-echo signals, T_1 leakage effects are minimal due to the use of a preload dose. T_1 leakage effects can be effectively removed for the dual-echo ΔR_2^*, and similar ΔR_2^* curves result from each injection in both the tumor ROI and AIF (note that the peak ΔR_2^* of the $1/2$-dose protocol is concomitantly reduced with the lower dose). In these examples, leakage correction removed residual T_2^* leakage effects for both dual-echo and single-echo protocols. The T_1-weighted signal resulting from the dual-echo extrapolation to TE = 0 is shown on the bottom row for each protocol.

Whole-brain tSNR and tumor CNR are shown in Figure 2 for each protocol. The basic protocol yielded

similar tSNR to the single-echo tSNR, likely due to the similarity between the protocols ($p = 0.910$). The $1/2$-dose dual-echo protocol yielded significantly lower tSNR compared to the single-echo tSNR ($p = 0.004$), due to lower contrast dose, as did the low FA and short TR protocols ($p < 0.001$ for both). Despite the lower whole-brain tSNR, the dual-echo and single-echo tumor CNR were not significantly different across all protocols (basic, $1/2$-dose preload, low FA, and short TR: $p = 0.188, 0.666, 0.059,$ and 0.688, respectively). For the single-echo acquisition, there was no significant difference across groups for tSNR or CNR ($F(3,55) = 0.011$ and $0.087, p = 0.998$ and 0.967, respectively). For dual-echo acquisitions, there was a significant group effect across protocols for tSNR ($F(3,55) = 7.84, p < 0.001$); significant differences were observed
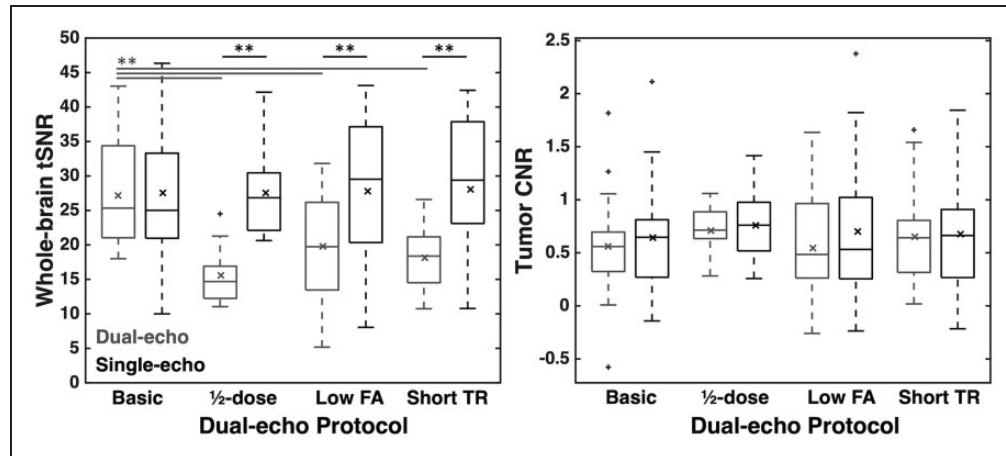
Figure 2. Whole-brain tSNR and tumor CNR across injections and protocols. Dual-echo and single-echo values are shown in gray and black, respectively. Horizontal bar in each boxplot indicates median value, while *x* marker indicates mean values. ** indicates $p < 0.01$ (black: between single- and dual-echo; gray: between dual-echo protocols).

between the basic protocol and all other protocols ($p = 0.001$, 0.013, and 0.001 for ½-dose, low-FA, and short-TR protocols, respectively). No tSNR differences were observed between the ½-dose, low-FA, and short-TR protocols ($p > 0.423$ for all); moreover, dual-echo CNR was not different across protocols ($F(3,55) = 0.357$, $p = 0.784$).

Figure 3 shows a representative T_1-weighted post-contrast image, dual-echo rCBV, single-echo rCBV, and the tumor voxel-wise correlation plots from each protocol. The rCBV maps from each injection demonstrate high similarity across protocols, despite varying contrast dose, FA, and TR. The largest slope is observed for the ½-dose protocol, while the slopes for the remaining protocols are closer to unity. The voxel-wise CCC for each patient is shown in the corresponding plots. Figure S1 (supplementary material) shows the corresponding dual-echo and single-echo rCBF maps, along with the tumor voxel-wise correlation plots. The dual-echo rCBF is higher than the single-echo rCBF, particularly for ½-dose protocol. As a result, the voxel-wise CCC is generally lower, while the Pearson's *r* values reflect a moderate linear correlation.

Correlation and Bland-Altman plots for mean rCBV, hot-spot rCBV, and mean rCBF in the tumor ROI across all 59 subjects are shown in Figure 4, with each color representing the protocol used. The corresponding mean tumor rCBV, slope and intercept (from Deming regression), and CCC values are shown in Table 2, along with the mean bias and limits of agreement (LoA) for each protocol. The lowest CCC was observed for the ½-dose protocol, which also exhibited the largest (negative) bias. This could be indicative of either lower SNR for the dual-echo rCBV or inadequate suppression of T_1 leakage effects in the

single-echo rCBV, both due to the use of a ½-dose preload injection during the dual-echo acquisition. The remaining protocols all had excellent agreement and smaller absolute bias. For the ½-dose protocol, rCBV was different between dual-echo and single-echo ($p = 0.010$), possibly attributed to the lower dose, while there was no significant difference between rCBV using single- and dual-echo acquisitions for the remaining protocols (basic, low FA, and short TR: $p = 0.39$, 1.00, and 0.44, respectively). For hot-spot analysis, the combined slope was 1.25 with a CCC of 0.81 and an overall negative bias of -0.86. In all cases, the dual-echo hot-spot rCBV was significantly different from single-echo hot-spot rCBV (basic, ½-dose, low FA, and short TR: $p = 0.001$, 0.010, 0.034, 0.018, respectively). The individual Pearson's *r* values were 0.96, 0.82, 0.98, and 0.83, respectively.

The dual-echo rCBF was similar or slightly higher than single-echo rCBF for each protocol (Figure 4), with significant differences observed in all protocols except low FA (basic, ½-dose, low FA, and short TR: $p = 0.007$, 0.004, 0.325, and 0.001, respectively). Lower CCC values were observed for the ½-dose and low FA protocols (Table 2), with similar CCC for the basic and short TR protocols; additionally, both basic and short TR protocols had slopes close to unity. The Pearson's correlation coefficients exhibited higher linear correlations (basic, ½-dose, low FA, and short TR: 0.98, 0.94, 0.93, and 0.97, respectively). There was an overall negative bias for rCBF, with a trend toward increasingly overestimated rCBF as rCBF increased. The ½-dose protocol had the most negative bias, consistent with rCBV, which is less likely related to T_1 leakage effects but may be indicative of reduced SNR associated with a lower bolus dose.
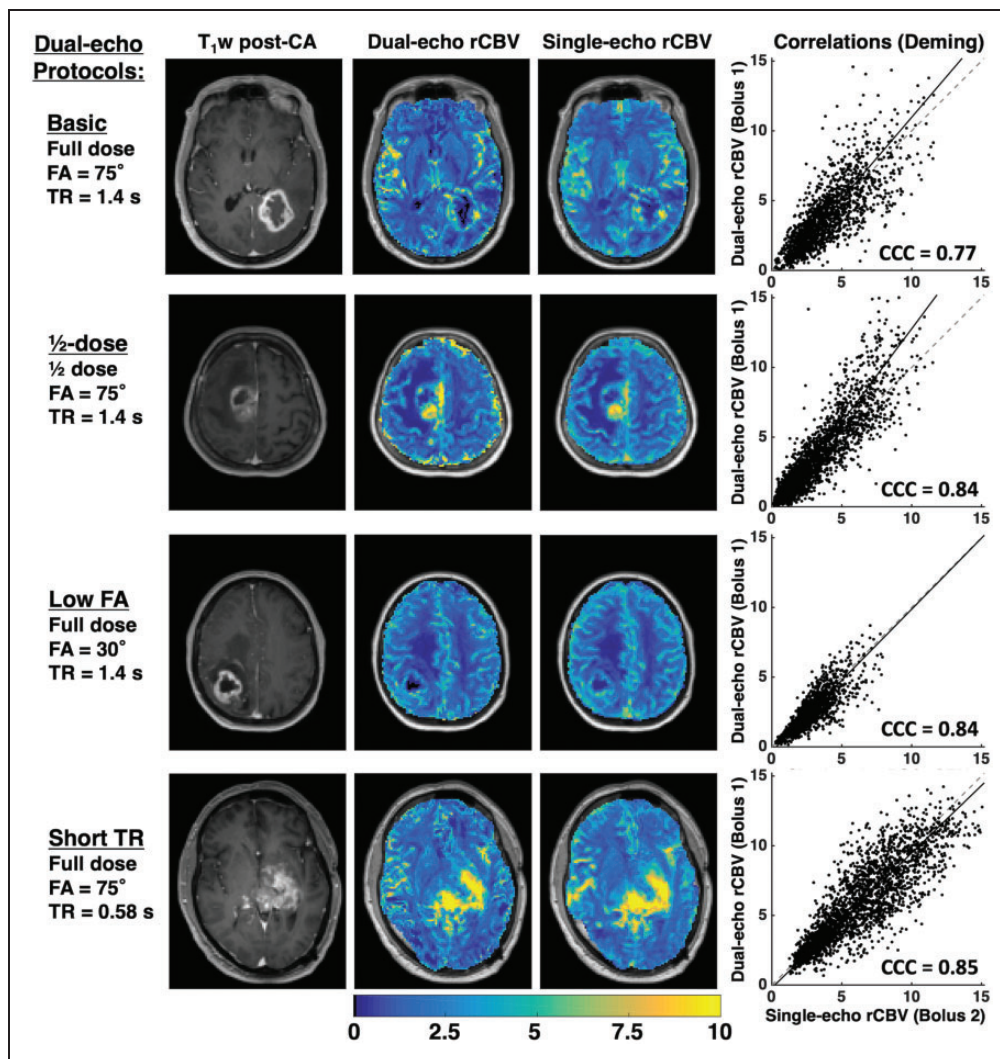
Figure 3. T$_1$-weighted post-contrast image, dual-echo and single-echo rCBV maps, and voxel-wise correlation plots for representative cases from each protocol. The correlation plots show the line of unity (dashed) and the best-fit line from Deming regression (solid line). The CCC is shown for each plot. All tumors shown are high-grade gliomas.

Figure 5 illustrates the combination of DSC-perfusion (specifically, rCBV) and DCE-permeability (specifically, K^{trans}) resulting from a single-bolus dual-echo perfusion strategy. Across all subjects, the mean (SD) K^{trans} values were 1.8 (0.6), 1.5 (0.6), 1.1 (0.5), and 2.1 (0.9) using basic, ½-dose, low FA, and short TR protocols, respectively (dual-echo rCBV values are given in Table 2). For dual-echo rCBV, there was no significant group effect across protocols (Kruskal-Wallis, $p = 0.190$); similarly, single-echo rCBV did not vary across the groups ($p = 0.557$). However, there was a significant group effect for K^{trans} across protocols (F $(3,55) = 5.77$, $p = 0.002$). Tukey post-hoc comparisons showed significant differences between basic and low FA protocols ($p = 0.048$) and between low FA and short TR protocols ($p = 0.001$).

Discussion

Two of the major challenges facing the DSC-MRI community are the need to develop perfusion workflows that yield highly accurate perfusion metrics across various sites and the need to reduce overall contrast agent dose. We have demonstrated that dual-echo acquisitions can produce comparable rCBV values to the standard double-dose protocols without the need for a preload, which can both simplify protocols across sites and reduce the patient contrast dose. Furthermore, for dual-echo protocols, the pulse sequence parameters (including TR and FA) were shown to have little impact on the resulting rCBV, allowing for significant flexibility in acquisition parameters.

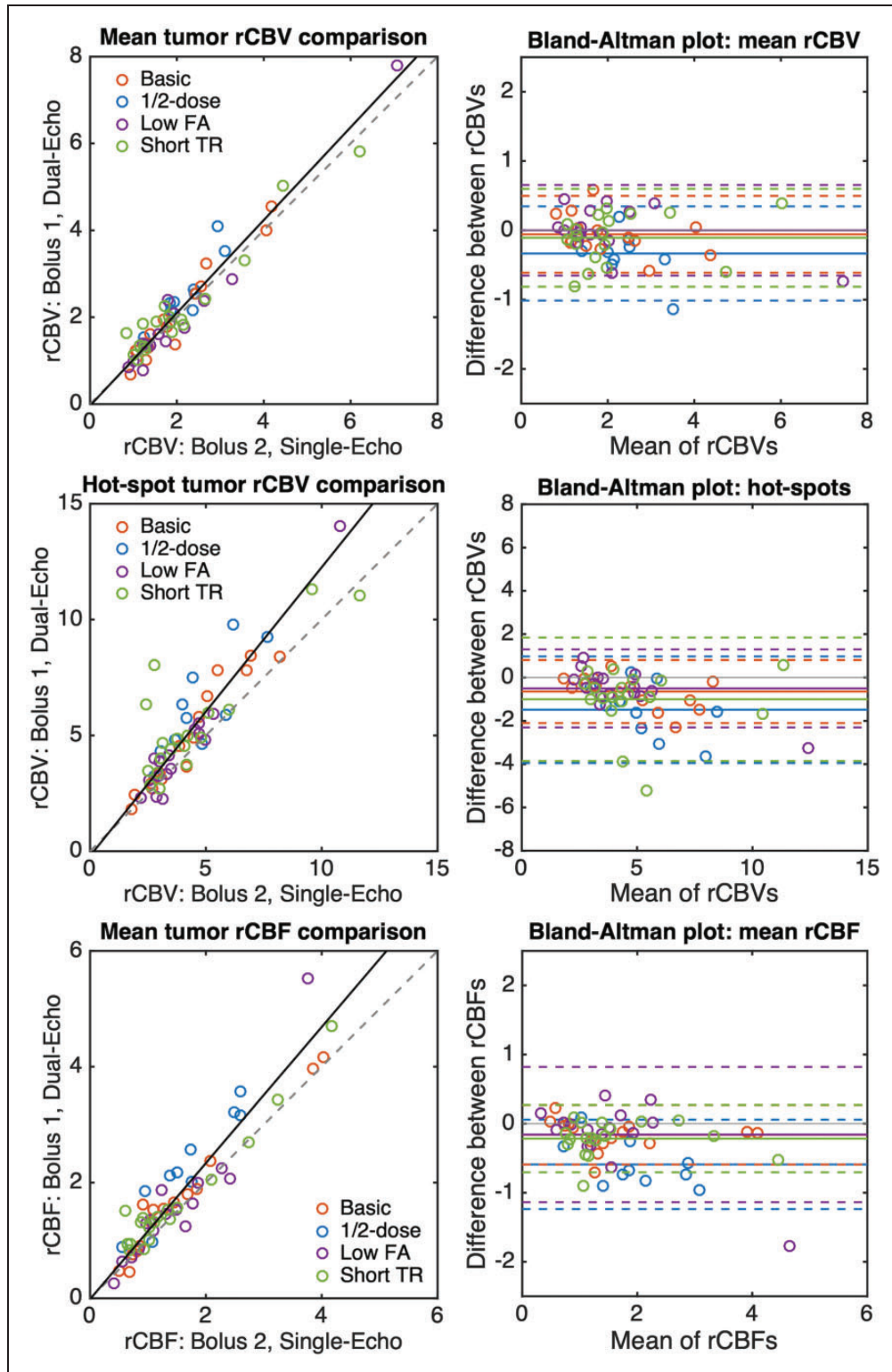As part of protocol harmonization efforts, we previously developed a DRO-based approach,[9,10] where

Figure 4. Correlation (left) and Bland-Altman (right) plots for mean tumor rCBV (top), tumor rCBV hot-spot (middle), and mean tumor rCBF (bottom). Colored circles represent the values from each patient with each protocol. The correlation plots show the line of unity (dashed) and the best-fit line from Deming regression (solid line) combining all protocols. The individual Deming regression results are shown in Table 2. Bland-Altman plots show the bias (solid line) for each protocol, along with the LoA (dashed lines).

Table 2. Mean (SD) tumor rCBV (top) and rCBF (bottom) for each injection (dual-echo and single-echo, respectively), along with slope, intercept, CCC, bias, and LoA for each protocol individually and pooled (ALL).

Dual-echo protocol	Dual-echo[a]	Single-echo[b]	Slope	Intercept	CCC	Bias	LoA
rCBV							
Basic	2.07 (1.13)	2.01 (1.01)	1.12	−0.18	0.96	−0.06	−0.61, 0.50
½-DOSE	2.47 (0.82)	2.14 (0.63)	1.34	−0.40	0.79	−0.33	−1.01, 0.34
LOW FA	2.02 (1.65)	2.02 (1.48)	1.12	−0.23	0.98	0.00[c]	−0.65, 0.65
SHORT TR	2.20 (1.29)	2.10 (1.38)	0.94	0.24	0.96	−0.11	−0.81 0.60
All	2.17 (1.28)	2.06 (1.20)	1.07	−0.04	0.96	−0.10	−0.78, 0.57
rCBF							
Basic	1.68 (1.11)	1.52 (1.08)	1.03	0.11	0.97	−0.16	−0.59, 0.27
½-DOSE	2.25 (0.90)	1.66 (0.72)	1.28	0.13	0.71	−0.59	−1.24, 0.06
LOW FA	1.62 (1.18)	1.62 (0.84)	1.44	−0.48	0.87	−0.16	−1.14, 0.82
SHORT TR	1.67 (1.00)	1.46 (0.99)	1.01	0.20	0.95	−0.22	−0.70, 0.27
All	1.76 (1.06)	1.51 (0.91)	1.17	−0.01	0.90	−0.25	−0.97, 0.47

[a]Dual-echo: Bolus 1.
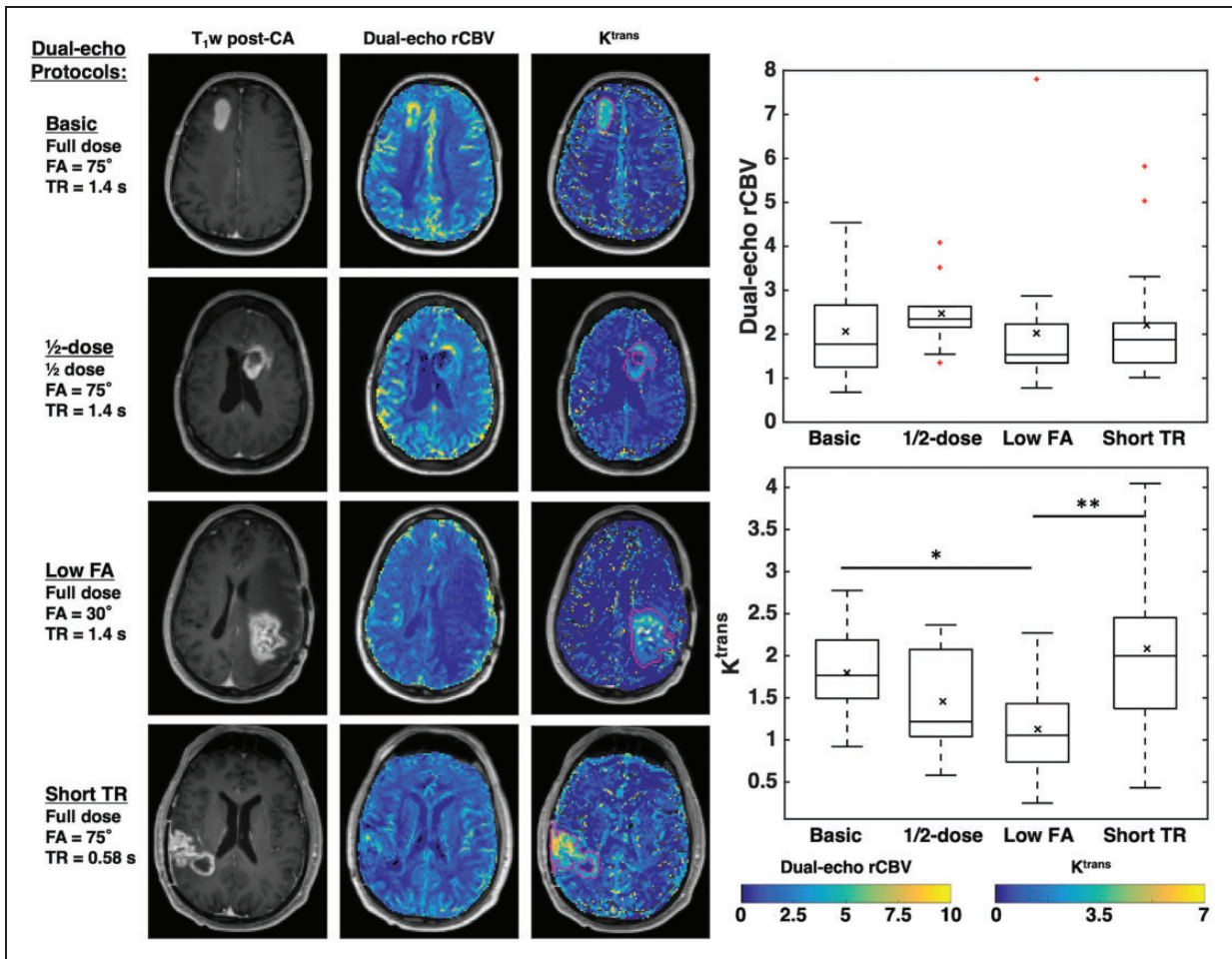[b]Single-echo: Bolus 2.
[c]4.19×10^{-4}.

Figure 5. Left: T_1-weighted post-contrast image, dual-echo rCBV maps, and maps of K^{trans} of representative cases from each protocol. All tumors shown are high-grade gliomas. Right: Boxplots showing dual-echo rCBV (top) and K^{trans} (bottom) values across protocols. Horizontal bar in each boxplot indicates median value, while x marker indicates mean values. * indicates $p < 0.05$, ** indicates $p < 0.01$.

the DRO was trained and validated using *in vivo* brain tumor patient data to yield a robust simulation dataset that enabled *in silico* testing of thousands of unique protocol combinations. This method revealed a single-dose protocol with high accuracy and precision based on a low-flip angle acquisition, which was recently validated by Schmainda et al.[11] However, the narrow parameter space over which low FA single-dose protocols yielded high rCBV accuracy led to the investigation of alternative approaches using multi-echo DSC-MRI,[16] which were shown *in silico* to yield high rCBV accuracy across TE combinations, TR, FA, dose, and field strength. The results of the present study verify our previous simulation results and demonstrate that dual-echo acquisitions obviate the need for preload dosing in a clinical setting with significant flexibility in acquisition parameters.

The dual-echo perfusion metrics in this study are compared to the corresponding double-dose single-echo perfusion metrics acquired in the same imaging session. To date, the double-dose protocol with a moderate flip angle has undergone extensive *in silico*, pre-clinical, and clinical validation and is widely recommended for DSC-MRI due to its high accuracy and clinical utility.[4,10,12,31,32] By nearly every metric used in this study, dual-echo single-dose perfusion performed comparably to single-echo perfusion with a preload (double-dose). Whole-brain tSNR was the most consistent between dual- and single-echo acquisitions using the basic dual-echo protocol, which is the most similar to the single-echo protocol. Using the low-FA single-echo protocol, Schmainda et al. found that normal-appearing gray matter had significantly lower tSNR, as measured directly from the single-echo signals, while tumor and NAWM were not significantly different.[11] Previous studies have observed reduced tSNR for short TR protocols in the context of functional MRI with SMS[33]; to account for differences in the number of acquired volumes (N), tSNR can be scaled by the square root of N, yielding the effective tSNR.[34] In this case, the effective tSNR for the short TR protocol was not significantly different from the single-echo protocol (data not shown). Despite these differences in tSNR across protocols, tumor CNR was not significantly different. Additionally, high correlations and low bias were observed for mean tumor rCBV using all dual-echo protocols compared to the standard single-echo mean tumor rCBV.

For mean tumor rCBV, the CCC for all dual echo protocols with a full dose was above 0.9, and Pearson's r ranged between 0.97-0.98, indicating both high precision and accuracy. While both CCC and Pearson's r were lower for hot-spot analysis, this may be partially indicative of the lower repeatability of hot-spot perfusion analysis[35] compared to the high repeatability of

mean tumor measurements.[36] For rCBF, dual-echo rCBF exhibited high precision (Pearson's r) but lower agreement (CCC). Interestingly, we observed that dual-echo rCBF had a slightly wider range than single-echo rCBF (maximum 5.3 and 4.2 for dual-echo and single-echo, respectively; similar minimum of 0.25 and 0.41, respectively). In our previous DRO-based simulations, we found that almost all protocols underestimated the true CBF, including the single-echo $1 + 1$ combination (serving as the reference standard here).[16] More specifically, the measured single-echo rCBF with preload (double-dose) was lower than dual-echo rCBF without preload (single-dose) across DRO parameter space, and dual-echo rCBF measurements were closer to the ground truth. This could indicate that single-echo rCBF may generally underestimate CBF, while dual-echo rCBF may be closer to the true CBF. One possible explanation is improved AIF quantification with dual-echo acquisitions.[20] However, for the $^1/_2$-dose preload protocol, the impact of lower tSNR may lead to reduced rCBF accuracy due to the smaller bolus dose (especially in white matter), while the short TR protocol may yield increased rCBF accuracy due to the higher sampling rate. These results are consistent with a previous simulation study by Knutsson et al. that showed increased CBF with increasing noise and negative CBF bias with higher TRs, with more accurate (higher) CBF with shorter TRs.[37]

For standard single-echo protocols, rCBV accuracy is reduced by T_1 and T_2^* leakage effects; dual-echo protocols are only impacted by T_2^* leakage effects. As T_1 leakage effects are removed from dual-echo perfusion metrics, there is considerably more flexibility in protocols. Both FA and TR do not impact dual-echo-derived perfusion metrics, beyond altering the relative image SNR and raw tSNR. In practice, image SNR could be improved by using an optimized FA, while shorter TRs may reduce CBF bias.[14,37] While only one TE combination was tested, we anticipate that a wide range of TE combinations will yield similar results, consistent with the DRO simulations.[16] The combination tested herein provided both a shorter TE and a longer TE more consistent with single-echo protocols. The inclusion of a first shorter TE did not significantly impact any of the pulse sequence parameters, beyond slightly increasing the longer TE (33.3 ms for dual-echo, *vs.* 30 ms for single-echo). Additional benefits of multiple echoes include improved AIF characterization[20] and higher rCBV accuracy for tissue components with a wide range of T_2^* values.[38] We also hypothesize that the inclusion of a shorter TE may improve quantification of perfusion metrics near susceptibility interfaces, which is relevant for tumors located in the inferior frontal and temporal lobes, as well as patients with shunts or large resection cavities.

Future work will assess this potential advantage of dual-echo perfusion protocols.

A potential advantage of dual-echo acquisitions is the opportunity to analyze individual echoes; for example, a secondary analysis (data not shown) was performed using the second echo (TE2) of the dual-echo acquisition, following the same procedure as the single-echo acquisition. Comparing mean tumor rCBV from TE2 to that of the single-echo rCBV, we found significant differences for the basic, $1/2$ dose, and short TR protocols ($p = 0.048$, 0.011, and 0.001, respectively). Consistent with the previous DRO[10] and *in vivo*[11] studies, the low-FA protocol did not show significant differences between TE2 single-dose rCBV and single-echo double-dose rCBV ($p = 0.383$). This further corroborates both the low FA approach and the protocol flexibility of dual-echo acquisitions to yield accurate rCBV measurements.

Furthermore, multiple echoes enable quantification of T_1 leakage effects, which can improve correction for residual T_2^* leakage effects[3] and permits simultaneous DCE analysis.[39–41] While both DSC- and DCE-MRI involve the use of exogenous gadolinium-based contrast agents, these methods differ in their dependence on relaxation effects (T_2^* and T_1, respectively), making simultaneous estimations of both perfusion and permeability incongruous using standard acquisitions.[42] Using dual-echo protocols, we have shown that rCBV accuracy is decoupled from FA and TR, over a wide range of TE combinations. This enables FA and TR to be optimized for high T_1 sensitivity, which is critical for accurate DCE modeling.[43] Of the protocols used in this study, the low FA protocol has the lowest sensitivity to T_1 effects (and yielded significantly lower K^{trans} values), while the short TR protocol has the highest sensitivity to T_1 effects. As reduced T_1 sensitivity may negatively bias the resulting K^{trans} values,[43,44] dual-echo protocols with higher T_1-weighting may provide a hidden advantage for simultaneous DCE and DSC measurements,[39] particularly given that similar rCBV accuracy can be achieved. For example, spiral trajectories provide an even shorter first TE,[45] and we anticipate spiral-based dual-echo methods will provide high rCBV accuracy, as well as increased T_1 sensitivity compared to EPI readouts.[46] Moreover, excellent agreement between dual-echo DSC-derived and standard DCE-derived K^{trans} measures was previously demonstrated in a preclinical study.[39] Undoubtedly, the ability to quantify complementary perfusion and permeability metrics in a single acquisition provides a more comprehensive tumor assessment.[42,47]

There are several limitations that are inherent in a retrospective study, including that the protocols were not prospectively assigned and that the datasets are limited to those available from institutional servers.

While data acquisition was not prospectively randomized for the dual-echo protocol, we do not anticipate that this would bias the results. Additionally, data for the $1/2$-dose protocol were only available from 10 subjects before full-dose preloads became standard-of-care, though the remaining protocols had data from 15-18 subjects. Some of the other limitations are the lack of ground-truth perfusion metrics, which would require alternative perfusion methods[48] or injection of non-gadolinium-based contrast agents that do not extravasate.[3,31] Another limitation is the use of a fixed T_1 value for the DCE-MRI analysis, as precontrast T_1 measurements were not available. Previous studies have shown that the use of a fixed T_1 value does not adversely impact diagnosis[29] and may actually be beneficial,[49] but it is acknowledged that a fixed T_1 could affect quantitative measures of K^{trans}. While this study was performed at 3 T, work is ongoing to assess dual-echo perfusion at 1.5 T, which our previous simulation study showed yielded higher accuracy.[16] Work is also ongoing to assess the impact of standardization, which has been previously shown to reduce the variability of rCBV measures,[50] and other post-processing methods.[51,52]

In conclusion, we have shown that the use of a single-dose, dual-echo DSC-MRI protocol gave comparable rCBV to single-echo DSC-MRI with a preload (double-dose) using *in vivo* data from brain tumor patients. This correlation was maintained across dosing, FA, and TR protocol variations. Dual-echo acquisitions provide significant pulse sequence flexibility and negate the need for a preload injection. This pulse sequence flexibility can further be leveraged to provide high T_1 sensitivity, thus enabling complementary assessment of both DSC perfusion and DCE permeability metrics in a single acquisition.

Declaration of conflicting interests

The author(s) declared no potential conflicts of interest with respect to the research, authorship, and/or publication of this article.

Authors' contributions

AMS and CCQ conceived of the idea. AMS analyzed data and wrote the paper. MB performed statistical analysis. LA aided in data analysis. LSH verified tumor regions of interest. LC Baxter, LSH, and JPK aided in implementation of protocols and in obtaining data for analysis. All authors provided critical feedback for the manuscript and aided in editing the manuscript.

ORCID iDs

Ashley M Stokes https://orcid.org/0000-0003-1137-5003
Laura C Bell https://orcid.org/0000-0001-8164-8324

Supplemental material

Supplemental material for this article is available online.

References

1. Boxerman JL, Schmainda KM and Weisskoff RM. Relative cerebral blood volume maps corrected for contrast agent extravasation significantly correlate with glioma tumor grade, whereas uncorrected maps do not. *AJNR Am J Neuroradiol* 2006; 27: 859–867.
2. Schmainda KM, Prah M, Connelly J, et al. Dynamic-susceptibility contrast agent MRI measures of relative cerebral blood volume predict response to bevacizumab in recurrent high-grade glioma. *Neuro Oncol* 2014; 16: 880–888.
3. Stokes AM, Semmineh N and Quarles CC. Validation of a T1 and T2* leakage correction method based on multiecho dynamic susceptibility contrast MRI using MION as a reference standard. *Magn Reson Med* 2016; 76: 613–625.
4. Welker K, Boxerman J, Kalnin A, et al.; American Society of Functional Neuroradiology MR Perfusion Standards and Practice Subcommittee of the ASFNR Clinical Practice Committee. ASFNR recommendations for clinical performance of MR dynamic susceptibility contrast perfusion imaging of the brain. *AJNR Am J Neuroradiol* 2015; 36: E41–51.
5. Schmainda KM, Prah MA, Rand SD, et al. Multisite concordance of DSC-MRI analysis for brain tumors: results of a national cancer institute quantitative imaging network collaborative project. *AJNR Am J Neuroradiol* 2018; 39: 1008–1016.
6. Hu LS, Baxter LC, Pinnaduwage DS, et al. Optimized preload leakage-correction methods to improve the diagnostic accuracy of dynamic susceptibility-weighted contrast-enhanced perfusion MR imaging in posttreatment gliomas. *AJNR Am J Neuroradiol* 2010; 31: 40–48.
7. Bell LC, Hu LS, Stokes AM, et al. Characterizing the influence of preload dosing on percent signal recovery (PSR) and cerebral blood volume (CBV) measurements in a patient population with high-grade glioma using dynamic susceptibility contrast MRI. *Tomography* 2017; 3: 89–95.
8. Semmineh NB, Xu J, Boxerman JL, et al. An efficient computational approach to characterize DSC-MRI signals arising from three-dimensional heterogeneous tissue structures. *PLoS One* 2014; 9: e84764.

9. Semmineh NB, Stokes AM, Bell LC, et al. A population-based digital reference object (DRO) for optimizing dynamic susceptibility contrast (DSC)-MRI methods for clinical trials. *Tomography* 2017; 3: 41–49.
10. Semmineh NB, Bell LC, Stokes AM, et al. Optimization of acquisition and analysis methods for clinical dynamic susceptibility contrast MRI using a Population-Based digital reference object. *AJNR Am J Neuroradiol* 2018; 39: 1981–1988.
11. Schmainda KM, Prah MA, Hu LS, et al. Moving toward a consensus DSC-MRI protocol: validation of a low – flip angle single-dose option as a reference standard for brain tumors. *AJNR Am J Neuroradiol* 2019; 40: 626–633.
12. Paulson ES and Schmainda KM. Comparison of dynamic susceptibility-weighted contrast-enhanced MR methods: recommendations for measuring relative cerebral blood volume in brain tumors. *Radiology* 2008; 249: 601–613.
13. Newbould RD, Skare ST, Jochimsen TH, et al. Perfusion mapping with multiecho multishot parallel imaging EPI. *Magn Reson Med* 2007; 58: 70–81.
14. Calamante F, Vonken EJ and van Osch MJ. Contrast agent concentration measurements affecting quantification of bolus-tracking perfusion MRI. *Magn Reson Med* 2007; 58: 544–553.
15. Stokes AM and Quarles CC. A simplified spin and gradient echo approach for brain tumor perfusion imaging. *Magn Reson Med* 2016; 75: 356–362.
16. Stokes AM, Semmineh NB, Nespodzany A, et al. Systematic assessment of multi-echo dynamic susceptibility contrast MRI using a digital reference object. *Magn Reson Med* 2020; 83: 109–123.
17. Boxerman JL, Schmainda KM and Weisskoff RM. Relative cerebral blood volume maps corrected for contrast agent extravasation significantly correlate with glioma tumor grade, whereas uncorrected maps do not. *Am J Neuroradiol* 2006; 27: 859–867.
18. Weisskoff RM, Boxerman JL, Sorensen AG, et al. Simultaneous blood volume and permeability mapping using a single Gd-based contrast injection. In: *Proceedings of the 2nd Annual Meeting of SMRM*, San Francisco, CA, USA, 6–12 August 1994. p. 279.
19. Liu H-L, Wu Y-Y, Yang W-S, et al. Is Weisskoff model valid for the correction of contrast agent extravasation with combined T[Sub 1] and T[Sub 2]*] effects in dynamic susceptibility contrast MRI? *Med Phys* 2011; 38: 802–809.
20. Newton AT, Pruthi S, Stokes AM, et al. Improving perfusion measurement in DSC-MRI through the use of multi-echo information for AIF determination. *AJNR Am J Neuroradiol* 2016; 37: 1237–1243.
21. Carroll TJ, Rowley HA and Haughton VM. Automatic calculation of the arterial input function for cerebral perfusion imaging with MR Imaging1. *Radiology* 2003; 227: 593–600.
22. Calamante F, Connelly A and Van Osch MJP. Nonlinear ΔR 2 * effects in perfusion quantification using bolus-tracking MRI. *Magn Reson Med* 2009; 61: 486–492.
23. Kjolby BF, Ostergaard L and Kiselev VG. Theoretical model of intravascular paramagnetic tracers effect on tissue relaxation. *Magn Reson Med* 2006; 56: 187–197.

24. Wu O, Stergaard L, Weisskoff RM, et al. Tracer arrival timing-insensitive technique for estimating flow in MR perfusion-weighted imaging using singular value decomposition with a block-circulant deconvolution matrix. *Magn Reson Med* 2003; 50: 164–174.

25. Liu H-L, Pu Y, Liu Y, et al. Cerebral blood flow measurement by dynamic contrast MRI using singular value decomposition with an adaptive threshold. *Magn Reson Med* 1999; 42: 1–6.

26. Barnes SR, Ng TSC, Santa-Maria N, et al. ROCKETSHIP: a flexible and modular software tool for the planning, processing and analysis of dynamic MRI studies. *BMC Med Imaging* 2015; 15: 19.

27. Tofts PS. Modeling tracer kinetics in dynamic Gd-DTPA MR imaging. *J Magn Reson Imaging* 1997; 7: 91–101.

28. Li X, Welch EB, Arlinghaus LR, et al. A novel AIF tracking method and comparison of DCE-MRI parameters using individual and population-based AIFs in human breast cancer. *Phys Med Biol* 2011; 56: 5753–5769.

29. Conte GM, Altabella L, Castellano A, et al. Comparison of T1 mapping and fixed T1 method for dynamic contrast-enhanced MRI perfusion in brain gliomas. *Eur Radiol* 2019; 29: 3467–3479.

30. Altman DG. *Practical statistics for medical research.* London: Chapman and Hall, 1991.

31. Boxerman JL, Prah DE, Paulson ES, et al. The role of preload and leakage correction in gadolinium-based cerebral blood volume estimation determined by comparison with MION as a criterion standard. *AJNR Am J Neuroradiol* 2012; 33: 1081–1087.

32. Prah MA, Stufflebeam SM, Paulson ES, et al. Repeatability of standardized and normalized relative CBV in patients with newly diagnosed glioblastoma. *AJNR Am J Neuroradiol* 2015; 36: 1654–1661.

33. Bhandari R, Kirilina E, Caan M, et al. Does higher sampling rate (multiband + SENSE) improve group statistics – an example from social neuroscience block design at 3T. *Neuroimage* 2020; 213: 116731.

34. Todd N, Moeller S, Auerbach EJ, et al. Evaluation of 2D multiband EPI imaging for high-resolution, whole-brain, task-based fMRI studies at 3T: sensitivity and slice leakage artifacts. *Neuroimage* 2016; 124: 32–42.

35. Smits M, Bendszus M, Collette S, et al. Repeatability and reproducibility of relative cerebral blood volume measurement of recurrent glioma in a multicentre trial setting. *Eur J Cancer* 2019; 114: 89–96.

36. Jafari-Khouzani K, Emblem KE, Kalpathy-Cramer J, et al. Repeatability of cerebral perfusion using dynamic susceptibility contrast MRI in glioblastoma patients. *Transl Oncol* 2015; 8: 137–146.

37. Knutsson L, Stahlberg F and Wirestam R. Aspects on the accuracy of cerebral perfusion parameters obtained by dynamic susceptibility contrast MRI: a simulation study. *Magn Reson Imaging* 2004; 22: 789–798.

38. Bell LC, Does MD, Stokes AM, et al. Optimization of DSC MRI echo times for CBV measurements using error analysis in a pilot study of high-grade gliomas. *AJNR Am J Neuroradiol* 2017; 38: 1710–1715.

39. Quarles CC, Gore JC, Xu L, et al. Comparison of dual-echo DSC-MRI- and DCE-MRI-derived contrast agent kinetic parameters. *Magn Reson Imaging* 2012; 30: 944–953.

40. Sourbron S, Heilmann M, Biffar A, et al. Bolus-tracking MRI with a simultaneous T1- and T2*-measurement. *Magn Reson Med* 2009; 62: 672–681.

41. Vonken E, van Osch M, Bakker C, et al. Simultaneous quantitative cerebral perfusion and Gd-DTPA extravasation measurement with dual-echo dynamic susceptibility contrast MRI. *Magn Reson Med* 2000; 43: 820–827.

42. Quarles CC, Bell LC and Stokes AM. Imaging vascular and hemodynamic features of the brain using dynamic susceptibility contrast and dynamic contrast enhanced MRI. *Neuroimage* 2019; 187: 32–55.

43. Schabel MC and Parker DL. Uncertainty and bias in contrast concentration measurements using spoiled gradient echo pulse sequences. *Phys Med Biol* 2010; 3: 1–19.

44. Dale BM, Jesberger JA, Lewin JS, et al. Determining and optimizing the precision of quantitative measurements of perfusion from dynamic contrast enhanced MRI. *J Magn Reson Imaging* 2003; 18: 575–584.

45. Paulson ES, Prah DE and Schmainda KM. Spiral perfusion imaging with consecutive echoes (SPICE) for the simultaneous mapping of DSC- and DCE-MRI parameters in brain tumor patients: Theory and initial feasibility. *Tomography* 2016; 2: 295–307.

46. Bell LC, Turley D, Semmineh NB, et al. Improving simultaneous T1 and T2* measurements for dynamic susceptibility contrast MRI using a 3D distributed spirals sequence. In: *Proceedings of the 25th Annual Meeting of ISMRM*, Honolulu, Hawaii, 22–27 April 2017. p. 1900.

47. Barbier EL, den Boer JA, Peters AR, et al. A model of the dual effect of gadopentetate dimeglumine on dynamic brain MR images. *J Magn Reson Imaging* 1999; 10: 242–253.

48. Noguchi T, Yoshiura T, Hiwatashi A, et al. Perfusion imaging of brain tumors using arterial Spin-Labeling: correlation with histopathologic vascular density. *AJNR Am J Neuroradiol* 2008; 29: 688–693.

49. Nam JG, Kang KM, Choi SH, et al. Comparison between the prebolus T1 measurement and the fixed T1 value in dynamic contrast-enhanced MR imaging for the differentiation of true progression from pseudoprogression in glioblastoma treated with concurrent radiation therapy and temozolomide che. *AJNR Am J Neuroradiol* 2017; 38: 2243–2250.

50. Bedekar D, Jensen T and Schmainda KM. Standardization of relative cerebral blood volume (rCBV) image maps for ease of both inter- and intrapatient comparisons. *Magn Reson Med* 2010; 64: 907–913.

51. Hu LS, Kelm Z, Korfiatis P, et al. Impact of software modeling on the accuracy of perfusion MRI in glioma. *AJNR Am J Neuroradiol* 2015; 36: 2242–2249.

52. Bell LC, Semmineh N, An H, et al. Evaluating multisite rCBV consistency from DSC-MRI imaging protocols and postprocessing software across the NCI quantitative imaging network sites using a digital reference object (DRO). *Tomography* 2019; 5: 110–117.